



**HAL**  
open science

## How chemical defects influence the charging of nanoporous carbon supercapacitors

Romain Dupuis, Pierre-Louis Valdenaire, Roland J.-M. Pellenq, Katerina Ioannidou

► **To cite this version:**

Romain Dupuis, Pierre-Louis Valdenaire, Roland J.-M. Pellenq, Katerina Ioannidou. How chemical defects influence the charging of nanoporous carbon supercapacitors. Proceedings of the National Academy of Sciences of the United States of America, 2022, 119 (17), 10.1073/pnas.2121945119 . hal-03920236v1

**HAL Id: hal-03920236**

**<https://hal.science/hal-03920236v1>**

Submitted on 31 May 2022 (v1), last revised 5 Feb 2024 (v2)

**HAL** is a multi-disciplinary open access archive for the deposit and dissemination of scientific research documents, whether they are published or not. The documents may come from teaching and research institutions in France or abroad, or from public or private research centers.

L'archive ouverte pluridisciplinaire **HAL**, est destinée au dépôt et à la diffusion de documents scientifiques de niveau recherche, publiés ou non, émanant des établissements d'enseignement et de recherche français ou étrangers, des laboratoires publics ou privés.

# How chemical defects influence the charging of nanoporous carbon supercapacitors

Romain Dupuis<sup>a,b,c</sup>, Pierre-Louis Valdenaire (the late)<sup>c</sup>, Roland J.-M. Pellenq<sup>c,d</sup>, and Katerina Ioannidou<sup>b,c</sup>

<sup>a</sup>IEM and ICGM, Univ. Montpellier, CNRS, Montpellier, France; <sup>b</sup>LMGC, Univ. Montpellier, CNRS, Montpellier, France; <sup>c</sup> MIT/CNRS/Aix-Marseille Université Joint Laboratory "MultiScale Materials Science for Energy and Environment", UMI MSE2, Massachusetts Institute of Technology, 77 Massachusetts Avenue, Cambridge, Massachusetts 02139, USA; <sup>d</sup>International Research Laboratory, EPIDAPO, CNRS-George Washington U., Washington DC

This manuscript was compiled on May 30, 2022

**Ion desolvation and confinement are key physical processes in porous-carbon based supercapacitors undergoing charging and discharging cycles. We investigate electrolyte interactions between polarized porous carbon with subnanometer pore sizes and aqueous sodium chloride electrolyte using molecular dynamics. Inspired by recent first principles calculations, we developed a scheme accounting for chemical defects in electrodes where only the non-sp<sup>2</sup> carbons species carry an extra negative charge (on the anode) and an extra positive charge (on the cathode) due to voltage polarization. This drives electrolyte species (ions and solvent molecules ; water in this work) to adsorb at the electrode surface and in subnanometric pores upon polarization. First we observe an asymmetrical desolvation process of sodium and chloride ions at the external surface of the electrodes. The ionic distribution at the external surface of the electrodes is consistent with the Debye-Hückel electric potential equation and empirical trends observed for non-porous electrodes. In a second stage, we demonstrate that the nanoporosity of the electrodes is filled with ions and scarce water molecules and contributes to about 20% of the overall capacitance. A fraction of desolvated ions are irreversibly trapped in the core of electrodes during discharge. While maintaining the overall electroneutrality of the simulation cell, we found that anodes and cathodes do not carry the same amount of ions at all time steps leading to charge imbalance.**

Ionic adsorption | Molecular dynamics | dehydration

Understanding ions in nano-confinement is the key element to get the fundamental physical basis of electrochemical energy storage underlying modern electrochemistry devices like batteries and supercapacitors (1, 2). In particular, fundamental understanding of the ionic adsorption processes and confinement inside nanoporous carbon electrodes is essential for predicting and improving the capacitance (3) or deionisation efficiency of carbon-based devices (4, 5). Recent in situ X-ray (6) and neutron scattering (7) have shown that subnanometric pores of carbon electrodes enhance the ionic adsorption and its overall capacitance performance (8). In fact, if the pores are of the same size as electrolyte ions, high capacitances (leading to the term supercapacitor) have been observed that does not follow existing theories and empirical trends (9–12).

The term of electrical double layer (EDL) capacitor comes from the classical picture of non porous electrodes that accumulate oppositely charged ions at their vicinity upon voltage polarisation in a mean-field dielectric continuum description of the solvent populated with point charged ions at a given concentration. This picture although very popular obviously does not hold for porous electrodes with sub nanometric pores. In particular, the mean-field Gouy–Chapman–Stern description of a EDL fails in high molar concentrations and for pore

sizes smaller than a few nanometers (typically 4 nm for carbon substrates) (13, 14). EDL predictions usually rely on the Poisson-Boltzmann theory and modified versions such as Debye-Hückel (15, 16) and Donnan models (17). More recent approaches based on thermodynamics theory for heterogeneous ionic fluids allow to take into account ionic size hence ionic position correlations(18). Recently, this statistical physics description of an EDL theoretical prediction was extended to include time dependence and study the dynamics of the ionic charging process of a planar electrode (19).

Presently, there is no theory capable of solving the electrostatics problem for ions confined in the nanopores of a disordered porous carbon material commonly used in electrochemical devices. Nowadays, atomistic simulation techniques implement statistical physics methods that are able of describing both the intrinsic textural disorder of a porous carbon materials at the nanoscale and the movement of electrolyte species (solvent molecules and ions) in their pores under operational functioning conditions of a supercapacitor device (i.e. under polarization) (20–23).

There are currently two main approaches to describe atomic systems under polarization, the constant voltage (CV) and the constant charge (CC) methods. (i) The CV approach assumes a perfectly conducting substrate hence accumulating/depleting charges only on the atoms at the pore and external surfaces with no regards to the intrinsically defective nature of porous

## Significance Statement

Nanoporous carbon texture makes fundamental understanding of the electrochemical processes challenging. Based on DFT results, the proposed atomistic approach takes into account topological and chemical defects of the electrodes and attributing them a partial charge that depends on the applied voltage. Using a realistic carbon nanotexture, a model is developed to simulate the ionic charge both at the surface and in the subnanometric pores of the electrodes of a supercapacitor. Before entering the smallest pores, ions dehydrate at the external surface of the electrodes leading to an asymmetric adsorption behavior. Ions in subnanometric pores are mostly fully dehydrated. The simulated capacitance is in qualitative agreement with experiments. Part of these ions remain irreversibly trapped upon discharge.

R.D, K.I, and R.P. designed, wrote the manuscript, discussed and analyzed the results, R.D. and P.-L. V. performed the calculations

Authors declare no competing interests.

<sup>2</sup>To whom correspondence should be addressed. E-mail: aikaterini.ioannidou@umontpellier.fr, romain.dupuis@umontpellier.fr

carbons (see Fig. 1(a)). Applied to porous carbon materials, the CV approach thus assumes that all carbon atoms are in the sp<sup>2</sup> hybridisation state, i.e. conducting electrons. The main assumption of the CV method is, therefore, the metallic approximation - the electrodes are considered ideal conductors with no localisation of electric charge except at the material boundaries in contact with the electrolyte. In recent simulation works(10), pore surfaces are treated as an extension of the external electrode surface. It is important to indicate that the charging process of substrate atoms is in the order of fs while ion diffusion occurs at the scale of ns (24, 25). Thus upon polarisation, the charges on the solid matrix species attract ions first. Once equilibrium is reached, thermal agitation of adsorbed ions can induce (in a constant voltage description) charge fluctuation on electrode atoms that in turn can redistribute ions in their vicinity. This is the main advantage of the CV approach; its main drawback is that it ignores charge localisation due to chemical heterogeneity. As a result, within the CV approach, ion docking is only observed at the external surfaces of the electrodes or in large nanopores; the subnanopores being found not to participate to the capacitance in sharp contrast to experiment of activated carbon based super-capacitors (see Fig. 1(b))(3).

(ii) The standard CC approach gives all substrate atoms the same fixed charge. The main drawback of the CC approach is that substrate charges are not allowed to fluctuate upon ion docking. Thus, this method only simulates the initial ion docking dynamics before charge self-regulation takes place. In the literature, it was reported that the CC approach may lead to an unphysical temperature increase(26). In the supplementary materials we give evidence that this issue might come from the configurational setup of the simulation cell with bouncing walls for ions in a rigid electrodes approximation. With a full periodic cell simulating a stack of immersed electrodes, using NVE simulation under polarization we found that the temperature was well tempered (after initial relaxation at 300K). However, this leads to unphysical ion docking deep in the electrodes regardless the pore size (see Fig. 1(b)). In sum, both the standard CC and CV methods fail for different reasons hence, are not able to reliably simulate the adsorption of ions in subnanoporous polarized electrodes (see Figs. 1(a, b)).

Therefore, we modified the CC method guided by experimental and theoretical results showing the key role of chemical defects and subnanopores in the building up of the capacitance(9, 27-34). With this method, there is no additional computational cost compared to classical MD-CC calculations. The local electrostatic field generated by the matrix defects (in the present work non sp<sup>2</sup>-carbon atoms and edge hydrogen species) drives ion adsorption on the electrode external surface as well as in the whole porosity including the subnanopores. Our electrodes are made of porous carbon texture that is found to be realistic for charcoal, activated carbon as well as for mature kerogen(35, 36). It was obtained using Hybrid reverse Monte Carlo(37) with a density around 1g/cc. Note that our activated carbon texture contains subnanometric pores of 0.5-0.9nm (see Fig. 1(d)). This sharply contrasts from Carbide-Derived-Carbons (CDC) (38) previously used in supercapacitor simulations that only contains pores above 1nm.

We propose a chemically driven charge localization model

(CDCL) that locates partial charges to defective species through the entire electrodes including species at the external or pore surface that are by nature defective. It takes advantage of both CC and CV methods while correcting their main drawbacks opening the path for modelling the adsorption of ions in subnanoporous defective electrodes including the role of doping of elements as such as N, S, F, etc.

We demonstrate that using MD simulations with the COM-PASS force field(39, 40) at 300K, the CDCL approach unravels many subnanometric features underlying the physics of ion docking in the charged electrodes ranging from the differentiated desolvation mechanism of cations with respect to anions and their asymmetric adsorption/desorption mechanism inside the nanopores. The pore size distribution shows a maximum at 0.5-0.6 nm (Fig. 1(d)). Sodium and chloride ions can only dock as single bare ions (i.e. unsolvated) in those pores. The electrodes are separated by 30Å on both sides. The system is periodic in all directions and it is initially prepared with 6100 water molecules, 60 sodium and 60 chloride ions in the inter-electrodes regions corresponding to a salt concentration of 0.67 mol/L (see Methods). As shown in Fig. 1(e), the texture of the electrode near the ions contains defects (incomplete rings or rings with 5 members). Fig.1(f) shows the ion density after polarization and we can observe ion docking inside the porous electrodes.

## 1. Results and discussion

In view of the limitations identified for the CC and the CV method, we have chosen to develop the CDCL approach guided by the chemical attributes of the electrodes. Our electrodes are made of 70% sp<sup>2</sup> carbon atoms i.e. having three carbon neighbors as immediate neighbors with a typical angle between consecutive carbon atoms around 120 degrees. The other 30% of carbon atoms can be considered as defects where charges are localised (an increase of partial charge for anode atoms, a decrease for cathode species) (41) (see DFT calculations in S.I.).

Upon polarization, DFT calculations show that excess charges in absolute value are localized on the defects or at their vicinity (30). Therefore, the CDCL scheme for the attribution of additional charges consists in applying a  $\Delta_q$  value to the non-sp<sup>2</sup> carbon atoms while attributing a null charge to sp<sup>2</sup> carbon atoms. The sp<sup>2</sup> character is hereafter determined based on the C-C-C angle between three consecutive carbon atoms (see S.I.). For the sake of simplicity, we assume the following linear formula for the excess charge estimate:

$$\begin{aligned} \Delta_q &= \Delta_{q,max} * (|\Theta - \Theta_{max}|/10) \forall \Theta \in [\Theta_{max} - 10, \Theta_{max} + 10] \\ \Delta_q &= \Delta_{q,max} \forall \Theta \notin [\Theta_{max} - 10, \Theta_{max} + 10] \end{aligned} \quad [1]$$

where  $\Theta_{max}$  is the value of the C-C-C angle in a perfect sp<sup>2</sup> matrix (equal to 120 degrees) and  $\Delta_{q,max}$  is the maximum excess charge (positive for the anode and negative for the cathode), which magnitude depends on the applied voltage. We calculated that a value of +/-  $\Delta_{q,max}=0.0337 e$  gives an excess/deficit average charge on the anode/electrode of  $\Delta_q$  equals +/- 0.02 e. In order to compare our results with results obtained with the CV method, we have calculated a conversion factor by computing the average charge attributed to the electrode atoms in the CV method. If we apply 1V, the

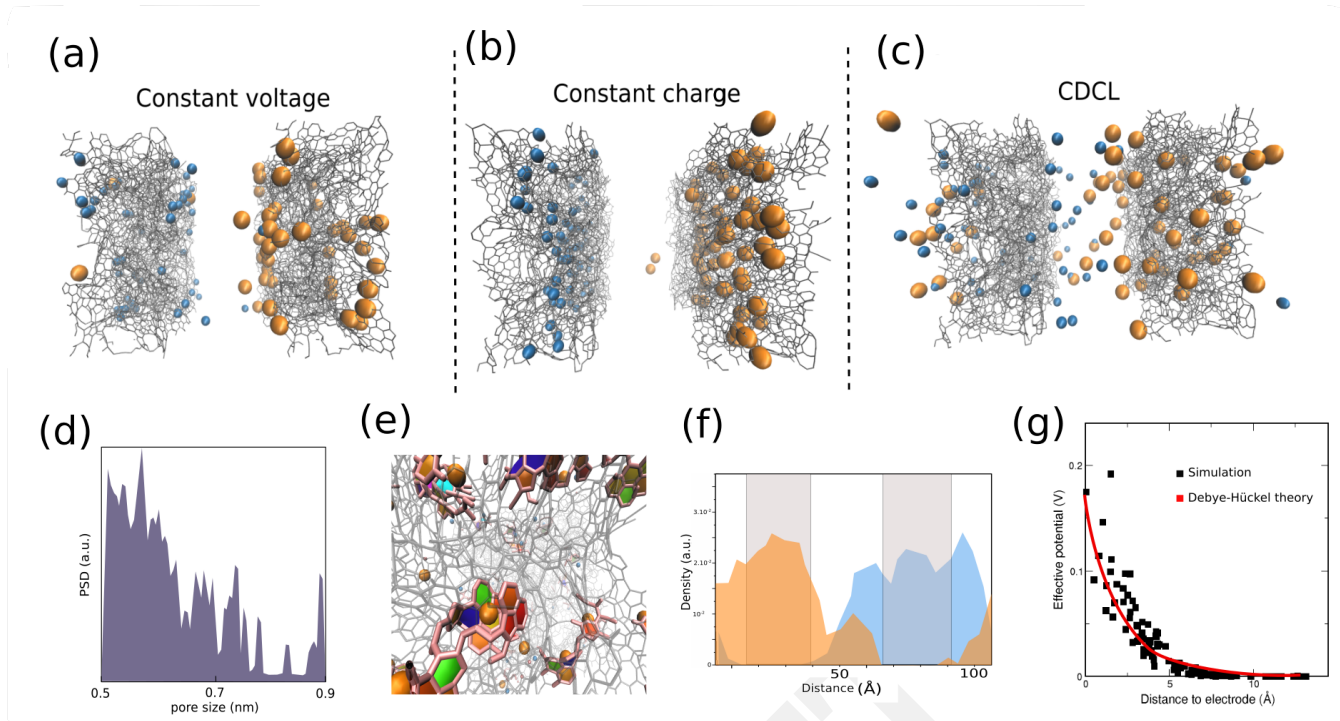


**Fig. 1.** (a,b and c) Snapshots of the system showing ionic adsorption in different polarisation schemes upon steady state for the constant charge, the constant voltage and the chemistry driven charge localisation schemes respectively. (d) Pore size distribution of the electrodes. (e) structure of the local structure of the porous carbon electrode near adsorption sites. Colored surfaces are guides for the eyes to emphasizing the texture of the pores near the docked-ions. (f) density of Na (in blue) and Cl (in orange) for  $\Delta_q = 0.02 e$  (1V) along the simulation cell axis, the two grey bands correspond to the electrodes position and thickness. (g) Calculation of the effective electrical potential acting on the ions in the solution for  $\Delta_q = 0.02 e$  (1V). Effective potential acting on the ions in the simulation cell (in black). Due to the roughness, the position of the surface has to be defined arbitrarily, which has been done using the position of the most forward carbon atom of the electrode. Fit obtained using the Debye-Hückel formula (in red). The charge distribution follows a Debye-Hückel law due to the screening of the solution.

170 average excess/deficit charge is  $\pm 0.02 e$  per carbon atom on  
 171 the anode/cathode respectively, which gives a voltage conversion  
 172 factor of 0.02. In the CDCL approach, carbon defective  
 173 species have a nominative charge that reflects their local chemi-  
 174 cal environment and is in absolute value proportional to the  
 175 departure from the perfect  $sp^2$  state (equation 1) and the  
 176 applied voltage.

177 Recent CV atomistic simulations of CDCs carbon-based  
 178 porous structures have shown that solvated ions are adsorbed  
 179 in pores above 1nm in size; no fully dehydrated ions have been  
 180 observed implying that the subnanopores are still empty, in  
 181 agreement with what we observe in our CV simulations(42).  
 182 As demonstrated here below, it is important to note that the  
 183 CDCL approach is the only method that is able to predict at  
 184 the same time the adsorption of fully dehydrated ions inside  
 185 the subnanopores (less than 1 nm, Fig. 1(c)), partially or fully  
 186 hydrated ions on the external surface or in any other kind of  
 187 larger pores. All confinement environments were experimen-  
 188 tally found to contribute to the overall capacitance of EDL  
 189 devices(2).

190 First, we investigate the adsorption of ions on the external  
 191 surface of the electrodes. The excess charge imposed additional  
 192 Coulombic forces on the ions of the system. The effective  
 193 voltage acting on the ions has been computed by extracting  
 194 the Coulombic forces on the ions with and without electric field  
 195 at the initial time of the simulation. The charge distribution,  
 196 in Fig. 1(g), shows that ions close to the external surface of the  
 197 electrodes are the ones experiencing larger attraction forces due

to the applied voltage compared to ions in bulk electrolyte away  
 from the electrode surface. Since it is related to a Coulombic  
 term, the force experienced by the ions is proportional to  $\Delta_q$   
 (see equation 1). The evolution of the effective potential is  
 characteristic of electrolyte solution and screening effect. Using  
 the Debye-Hückel formula(43), we can compare the Debye  
 length obtained from the simulation and that for a solution  
 with a uniform ion distribution for an ionic concentration of  
 $0.67 \text{ mol.L}^{-1}$  (corresponding to the salt concentration in  
 the inter-electrode void), with a dielectric constant of 80(44).  
 The agreement between the simulation and the Debye-Hückel  
 expression for the electric potential at the external surface  
 of the anode is remarkably good and gives a Debye length  
 around 0.2-0.3 nm in quantitative agreement with Debye length  
 obtained for this electrolyte type and concentration(44).

The number of effective ions adsorbed on and in both porous  
 electrodes is related to the capacitance of the system. The  
 capacitance has been calculated and is reported on Fig 2(a) for  
 each simulation with different  $\Delta_q$  (the estimation of voltage is  
 given from the aforementioned conversion). There is a thresh-  
 old at low voltage above which ions are being adsorbed on the  
 external surface of the electrodes (approximately  $\Delta_q=0.0025 e$   
 corresponding to 0.125 V). For larger polarization voltages,  
 the amount of ions incorporated in the electrodes increases  
 quasi-linearly until it reached the maximum, hence, the capaci-  
 tance exhibits a peak shown in Fig. 2(a) in agreement with  
 the recent theoretical and simulation work of Verkholyak et  
 al.(45). Note that at voltages above about 1.8V, we consider

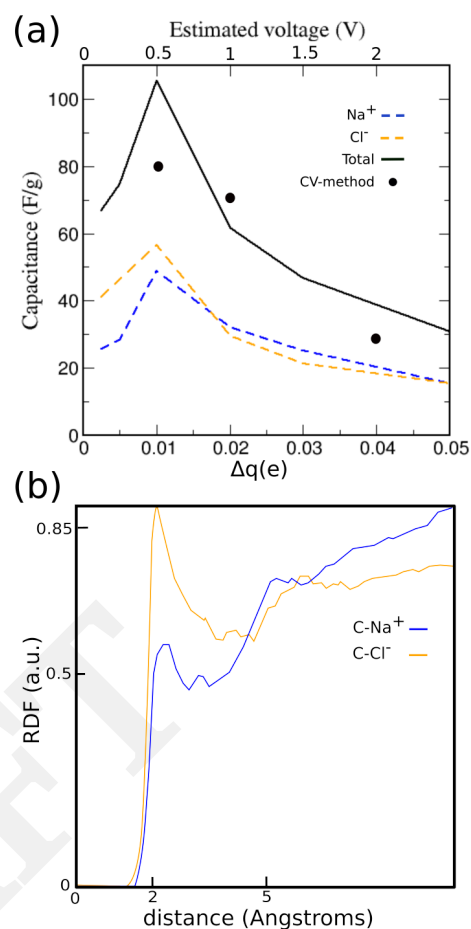
226 that the simulation is probably unrealistic since we do not  
 227 consider water splitting that happens at these voltages(46).  
 228 The capacitance is in agreement with the typical measured capac-  
 229 itance of activated carbons (around 100 F/g with a specific  
 230 surface area at around 500 m<sup>2</sup>/g for our carbon texture) (47).  
 231 The maximum capacitance we find, of about 20μF/cm<sup>2</sup> is in  
 232 agreement with experimental values (2, 9, 10). Comparing the  
 233 results obtained with the CV and the CDCL on figure 2(a), we  
 234 can estimate that the contribution of the subnanopores to the  
 235 capacitance is about 20%, meaning that the supercapacitor  
 236 made of subnanoporous electrodes remains mostly a standard  
 237 EDL device with respect to aqueous electrolytes.

238 Due to the ionic docking in the subnanometric pores, the  
 239 capacitance estimated from the CDCL method is larger than  
 240 that the one obtained with the CV method (dots, see Fig. 2(a)).  
 241 There is a positive correlation between the capacitance and  
 242 the specific surface area as measured with BET experiments  
 243 (48). In fact the large value of the specific surface area reflects  
 244 both the amount of subnanopores and chemical defects on the  
 245 carbon backbone. Chloride and sodium contribute differently  
 246 to the capacitance (orange and blue dashed lines, see Figs.  
 247 2(a)). The adsorption sites are different due to the ionic  
 248 size, as shown by the radial distribution function in Fig 2(b).  
 249 This leads to an asymmetric loading and charge unbalanced  
 250 electrodes, which is a direct consequence of the ion docking  
 251 into the subnanometric pores (while the simulation cell overall  
 252 charge remains neutral at all times in the simulation). The  
 253 capacitance being the sum of the charges divided to the voltage,  
 254 the peak can be explained with the less and less efficient ion  
 255 docking upon voltage increase, this will be discussed hereafter.

256 In more detail, Figs. 3(a) and (b) show the number of  
 257 adsorbed ions on the surface, inside the subnanopores of the  
 258 electrodes during polarization simulations and the total ionic  
 259 loading during charge and discharge simulations with  $\Delta_q =$   
 260 0.01e (see S.I. video). At the voltage corresponding to the max-  
 261 imum capacitance, the total adsorption is larger for Cl<sup>-</sup> than  
 262 Na<sup>+</sup>. Comparing Figs. 3(a) and (b), one can see that Na<sup>+</sup>  
 263 is mostly adsorbed at the external surface whereas Cl<sup>-</sup> is equally  
 264 adsorbed inside and at the external surface of the electrodes.  
 265 We observe that half of the sodium ions are adsorbed; the rest  
 266 remains in the solution in-between the electrodes. Similarly,  
 267 2/3 of the chloride ions are adsorbed and 1/3 remain in the  
 268 electrolyte solution.

269 Fig. 3(c) shows the number of adsorbed ions (i) on the sur-  
 270 face, (ii) inside the nanopores and (iii) in total for different pol-  
 271 arizations. Cl<sup>-</sup> ions are partially adsorbed on the surface and  
 272 inside the electrode nanopores following a monotonous increase  
 273 until  $\Delta_q=0.01e$  (0.5V) and then it reaches a plateau. Na<sup>+</sup>  
 274 is adsorbed in larger quantity than Cl<sup>-</sup> at voltages larger than  
 275  $\Delta_q=0.01e$  (0.5V). Interestingly, as the voltage increases, we  
 276 observe a transition from an external surface adsorption only  
 277 (from  $\Delta_q=0.0025e$  to  $\Delta_q=0.01e$ ) to a dual inside-pore dock-  
 278 ing/surface adsorption for the sodium ions above  $\Delta_q=0.01e$   
 279 (0.5V). This is due to the fact that surface adsorption involves  
 280 hydrated ions whereas inside-pore docking involves bare ions.  
 281 Low voltages do not provide enough energy to loosen the hydra-  
 282 tion shell of Na<sup>+</sup> leading to external surface adsorption of  
 283 hydrated ions (2).

284 The process of ion adsorption in nanopores is accompanied  
 285 with a change in the solvation shell of the ions. In bulk water,  
 286 sodium ions have a first solvation shell made of approximately 6



287 **Fig. 2.** (a) Capacitance due to sodium and chloride ions adsorbed inside and  
 288 onto the electrodes at steady state with a maximum additional charge  $\Delta_q$  (the  
 289 added/subtracted charge is maximal on defective (non-sp<sup>2</sup>) sites). Note that the  
 290 carbon atoms at the vicinity of the pores are not necessarily the non-sp<sup>2</sup> carbons. The  
 291 x-axis represents the excess of charge on each carbon atom of the positive electrode  
 292 with respect to  $\Delta_q$ . The dots correspond to the calculated value with the CV method.  
 293 The simulated capacitance value is in the ballpark of experimental values (100 F/g)  
 294 for supercapacitors based on porous carbons with specific surface area around 500 m<sup>2</sup>/g  
 295 (which is the value of our simulated porous carbon) (b) Radial distribution functions  
 296 for C-Na and C-Cl distances at steady state for  $\Delta_q = 0.01e$ .

287 water molecules (49), which is also observed in our simulations  
 288 before charging the electrodes. An ion and its first layer  
 289 hydration shell are of about 0.7 nm in diameter and, therefore,  
 290 can only access the largest pores in our system.

291 Fig. 3(d) shows the evolution of the hydration shells of the  
 292 adsorbed Na<sup>+</sup> and Cl<sup>-</sup> ions together with the total number of  
 293 adsorbed ions at  $\Delta_q=0.01e$  (0.5V). The adsorbed Na<sup>+</sup> ions are  
 294 surrounded on average by 4-5 water molecules, whereas the  
 295 Cl<sup>-</sup> ions carry 2-3 water molecules. All adsorbed ions have lost  
 296 either partially or totally their hydration shell, when adsorbed  
 297 on the surface of the electrodes, or their whole hydration shell  
 298 when entering the subnanopores. Fig. 3(e) shows the hydration  
 299 number of Cl<sup>-</sup> ions before adsorption and after adsorption  
 300 inside the nanopores. The hydration shell becomes loose at  
 301 the surface and then the ions can enter either bare or with at  
 302 most one water molecule in the subnanopores. Note that we  
 303 observed the formation of anion-cation ionic pairs only in the  
 304 solution outside of the electrodes.

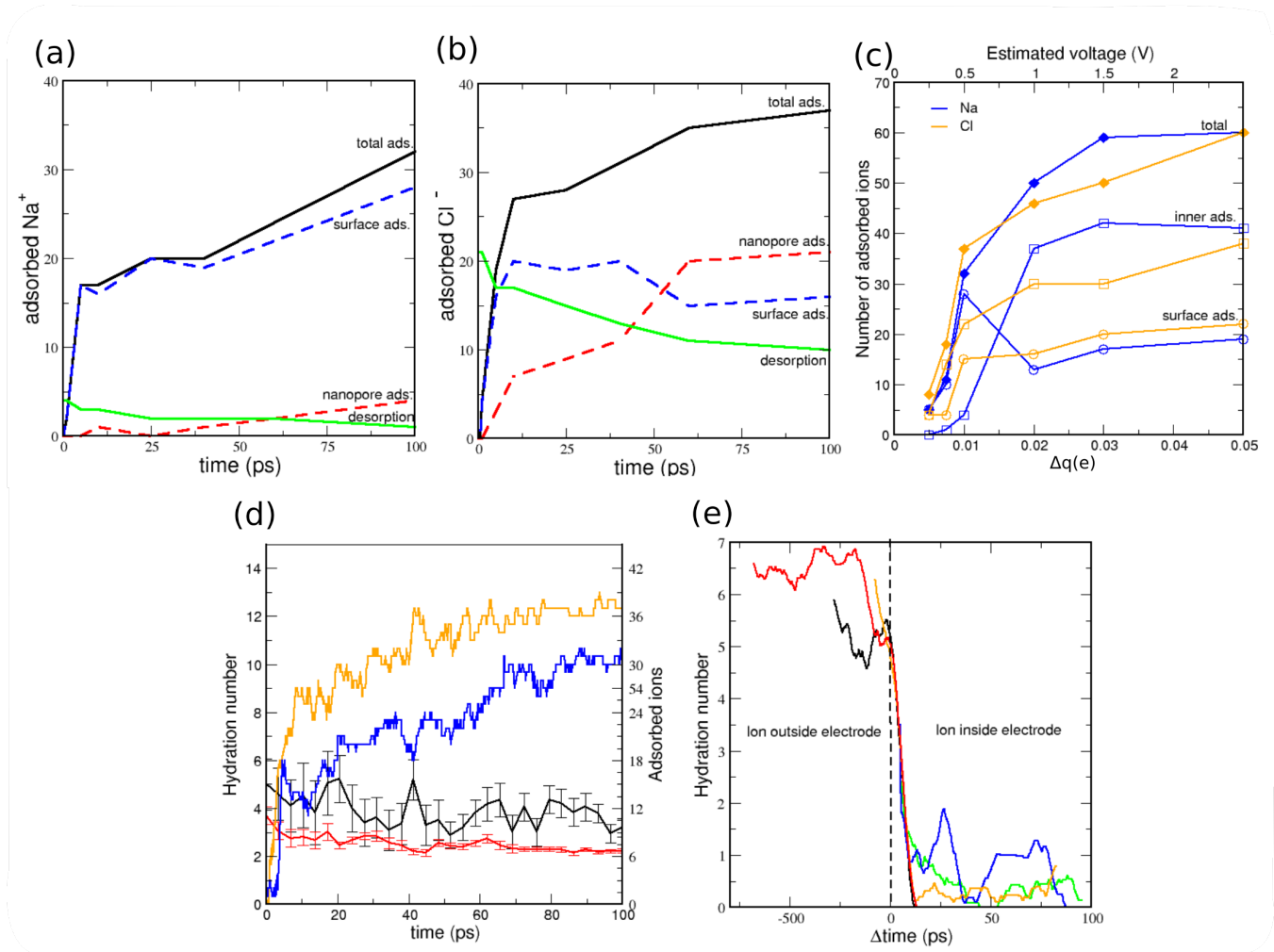


**Fig. 3.** (a) Evolution of the number of sodium ions in the electrode during the loading, adsorbed in the pore network (blue) or on the surface of the electrode (red) while imposing a voltage corresponding to a  $\Delta q = 0.01e$  (0.5V) (total in black) and during unloading (in green) for  $\Delta q = 0$ . To determine the adsorption, a cutoff of 4.0 Å and 5.0 Å have been used for Na-C and Cl-C distances respectively, corresponding to the first minimum in the radial distribution functions. (b) Evolution of the number of chloride ions in the electrode. (c) Number of (blue) sodium ions and (orange) chloride ions adsorbed (diamond) in total, (squares) inside the electrodes, (circles) at the surface. (d) Evolution of the hydration number during the adsorption around Na (black) and Cl (red) ions and number of ions adsorbed inside the electrodes at  $\Delta q = 0.01e$  (0.5V). Error bars correspond to the standard deviation. Evolution of the quantity of adsorbed Na (blue) and Cl (orange). (e) Hydration number of several ions versus  $\Delta \text{time}$  (each color corresponds to a different  $\text{Na}^+$  ion), where  $\Delta \text{time}$  is the time difference to the moment where the ion enters into the electrode. The values reported are the running average over 100 steps.

305 Focusing now on the role of water in porous electrodes at  
 306 full saturation, we observed that in polarized electrodes that  
 307 few water molecules adsorb in the pores of the electrodes (50).  
 308 The ratio for the amount of water inside the electrode is less  
 309 than 15%. The carbon structure is rather hydrophobic as  
 310 indicated by radial distribution functions (shown in S.I.), the  
 311 shortest C-water distance being about 3.5 Å .

312 Corrected for the effective accessible pore volume, the sub-  
 313 nanopores are just large enough to accommodate one bare ion  
 314 (diameter for sodium and chloride equal 0.1nm and 0.18nm  
 315 respectively) in agreement with the conclusions of Simon and  
 316 Gogotsi(2). While the electrodes are being charged, the den-  
 317 sity of water inside the electrodes slightly increases. This  
 318 indicates that the adsorption of ions into the carbon electrodes  
 319 make the structure less hydrophobic in a similar fashion as  
 320 the clay interlayer void is hydrophilic only because the pres-  
 321 ence of cations compensating the overall clay layer negative  
 322 charge. The clay basal planes per se are rather hydrophobic

323 as they carry no OH surface groups immediately in contact  
 324 with adsorbed water; the ions act as water pump inside a  
 325 polarized porous carbons or in-between clay layers charged  
 326 through isomorphic substitutions (51).

327 In summary, chloride and sodium ions in water are behaving  
 328 differently upon working conditions of a supercapacitor (52).  
 329 Chloride species appear to be more mobile than sodium ions  
 330 that are likely to get trapped in their tighter hydration cage  
 331 (53). It also makes chlorides adsorbing faster and at lower  
 332 voltage inside the carbon nanopores (see Figs. 3(a) and (b)).

333 Regarding the desorption process, the ions that are ad-  
 334 sorbed deep in the core of the electrode will more likely remain  
 335 trapped upon discharge. At voltage set back to zero, about  
 336 10% of the formerly docked  $\text{Na}^+$  ions (about 3% of the total  
 337 number of cations) and 30% of the adsorbed  $\text{Cl}^-$  (about  
 338 10% of the total number of anions) are still trapped inside  
 339 the electrodes (after 1 ns of unloading, 2  $\text{Na}^+$  and 6  $\text{Cl}^-$  are  
 340 inside the electrodes, see S.I.). Note that desorption, which is

341 simulated under a null voltage, takes place over a longer time  
342 than ion docking (see Figs. 3(a and b)). The trapped ions may  
343 not participate to the current unloading cycle but they could  
344 move to a nearby pore during the cycling and become again  
345 available for storage. The trapped ions upon depolarization  
346 is compatible with the hysteretic behavior observed in the  
347 supercapacitor I-V characteristic curve. More specifically, the  
348 ions that are being desorbed at zero voltage are only the ions  
349 that have an easy path to exit the porous material. Other  
350 ions, that are in small pores or in tortuous porous network,  
351 are not easily extracted from the media. Being smaller ion,  
352  $\text{Na}^+$  is often trapped more deeply in the porous network at  
353 larger voltages. Three adsorption/desorption cycles has been  
354 performed in this work and we have observed that after the  
355 first cycle, the amount of ions irreversibly docked inside the  
356 electrode nanoporosity remains constant.

## 357 2. Conclusion

358 We propose a new approach to describe the charge and dis-  
359 charge process in subnanoporous carbon made electrodes, in a  
360 supercapacitor setting, that we call chemically driven charge  
361 localisation model (CDCL). Despite its mean-field charac-  
362 ter, the CDCL approach is an improvement of the current  
363 standard methods to simulate charged devices at the atomic  
364 scale, namely the constant charge and the constant voltage  
365 methods that are ineffective to correctly describe ionic dock-  
366 ing in subnanopores. Informed from DFT calculations, the  
367 CDCL method consists in localising charges on defective non-  
368 sp<sup>2</sup> carbon sites, including chemical or topological defects.  
369 By contrast to the standard methods, this allows simulat-  
370 ing both adsorption on the electrodes external surfaces and  
371 in-subnanopore docking.

372 Applied to a realistic texture of nanoporous carbon, we  
373 could unravel the fundamental processes underlying the capac-  
374 itive effect of a subnanoporous carbon-based supercapacitor  
375 device in operation. We show in particular that subnanomet-  
376 ric pores constitute about 20% of the capacitance of such a  
377 device using a standard aqueous electrolyte. The simulated  
378 value of the capacitance of about 100 F/g (or 20  $\mu\text{F}/\text{cm}^2$ )  
379 is in good agreement with the experimental values measured  
380 on activated carbon based supercapacitors. In more details,  
381 we show that the docking of ions in pores is preceded by an  
382 assymetrical desolvation at the vicinity of the external pore  
383 surface. The ion adsorption density profile on the electrodes  
384 external surfaces is in agreement with the Debye-Hückel theory  
385 with a Debye length of 0.2-0.3nm. The desolvation process  
386 is actually different for sodium and for chloride ions as the  
387 hydration shell of sodium is tighter than that of chloride. Once  
388 ions are desolvated, they can access nanopores; subnanopores  
389 being mostly populated with bare ions in agreement with in  
390 situ X-rays experiments (6). Due to the difference in their  
391 ionic size, the docking mechanism of sodium and chloride ions,  
392 leads to an unbalanced electrode charging. Upon discharge, we  
393 found that a significant amount of ions (10% of the cations and  
394 30% of the anions) remains trapped in the subnanopores due  
395 to the pore network tortuosity right after the first charge that  
396 is compatible with the typical I-V curve of supercapacitors.

397 The current CDCL method allows exploring how doping  
398 with elements such as N, S, etc. influence the ion adsorption  
399 and the in-pore docking(54). Furthermore, the current CDCL  
400 method could be coupled with a constant voltage approach in

order to take into account the variation of the substrate defects  
charge upon ionic thermal movement. This will allow studying  
the ageing of the electrodes texture upon charge-discharge  
cycling.

## 3. Methods

401 A super-capacitor composed by porous carbon layers (of 22Å thick-  
402 ness), separated with a water solution containing electrolytes, has  
403 been simulated with a fully atomistic approach. The electrodes has  
404 been generated using a liquid quench MD method (55) using the  
405 reactive force field ReaxFF (56) to obtain a micro-porous carbon  
406 containing hydrogen (0.3 H/C). The charges due to defects in the  
407 carbon structure are compensated by H atoms. This structure has  
408 been relaxed at 293 K and 1 atm, then, cut in half in order to add  
409 a phase of bulk of water replacing the other half. The cut leads  
410 to unstable atoms at the interface due to broken bonds. Thus, we  
411 performed a relaxation with an MD run at a higher temperature  
412 (1500 K) to force water molecules to react with the unstable carbon  
413 atoms, stabilize the structure and diffuse within the structure. Then,  
414 we have duplicated the system one time toward the orthogonal di-  
415 rection of the cut surface. Each electrode contains 5440 atoms. It  
416 has a connected pore network and a density of 1.45  $\text{g}\cdot\text{cm}^{-3}$ .  
417

418 In order to study the charge of the capacitor with ions we have  
419 built a model in which pure water solution has been enriched with  
420 60  $\text{Na}^+$  and 60  $\text{Cl}^-$  ions. We have investigated the adsorption of  
421 the ions in the porous carbon structure that has been described  
422 previously. Since ReaxFF is not well suited for simulating systems  
423 with electric fields, the potential used for the charge and discharge  
424 simulations is the COMPASS potential (39, 40) to describe the  
425 electrodes-water interactions and the SPC/E (57) potential to de-  
426 scribe water molecule interactions which is well-known for its good  
427 description of polar liquids. The interactions cutoff has been set to  
428 12Å. In this work, considering the complexity of the electrodes and  
429 therefore of finding a relevant force field to simulate the motion of  
430 the atoms of the electrodes, the electrodes were kept rigid. This is  
431 an approximation that could slightly influence the quantity of ions  
432 that can be adsorbed (in a flexible system, one can imagine that  
433 the pores will slightly adapt to the presence of ions). In further  
434 studies, the use of reactive force fields such as ReaxFF should be  
435 considered in order to assess the stability of the structure and the  
436 durability of the pore network due to the ion adsorption. Since  
437 such a reactive potential relies on the calculation of charges at each  
438 step of the dynamics, the CDCL method should be implemented  
439 as a post-calculation to add the charge excess/deficit after the  
440 electronegativity equalization method algorithm.

441 Ewald summation has been used for the long range interactions.  
442 The PPPM scheme, which is well suited for large systems (in this  
443 work over 30 000 atoms), as implemented in LAMMPS has been  
444 used with a threshold on the forces of  $10^{-4}$ . Periodic boundary  
445 conditions have been imposed to the simulation cell. The electrodes  
446 are symmetrical and the simulation cell is electroneutral.

447 For the dynamics, we have used a time step of 0.2 fs, in agree-  
448 ment with the frequency of the O-H stretching modes in water.  
449 The system has been thermostated using Nosé-Hoover thermostats.  
450 Before adding the electric field, the system has been equilibrated  
451 during 300ps at 300K. As discussed in S.I., we have not observed  
452 any increase of temperature under electric field contrarily to the  
453 results published in a recent work by Merlet et al. (26) the authors  
454 attribute to a macroscopic dipole moment, which is an artifact of  
455 the simulation.

**ACKNOWLEDGMENTS.** R.D, P.-L. V and K.I have been sup-  
ported from the CNRS Momentum grant CEMCAP. Computations  
have been performed on the GENCI/CINES clusters withing the  
project A0090911009.

- 464 1. S Chu, A Majumdar, Opportunities and challenges for a sustainable energy future. *Nature* 488, 294–303 (2012).
- 465 2. P Simon, Y Gogotsi, Materials for electrochemical capacitors. *Nat. Mater.* 7, 845–854 (2008).
- 466 3. F Béguin, V Presser, A Balducci, E Frackowiak, Carbons and electrolytes for advanced supercapacitors. *Adv. Mater.* 26, 2219–2251 (2014).
- 467 4. S Porada, R Zhao, A [van der Wal], V Presser, P Biesheuvel, Review on the science and technology of water desalination by capacitive deionization. *Prog. Mater. Sci.* 58, 1388 – 1442 (2013).
- 468
- 469
- 470
- 471

- 472 5. ME Suss, et al., Water desalination via capacitive deionization: what is it and what can we  
473 expect from it? *Energy Environ. Sci.* **8**, 2296–2319 (2015).
- 474 6. C Prehal, et al., Quantification of ion confinement and desolvation in nanoporous carbon  
475 supercapacitors with modelling and in situ x-ray scattering. *Nat. Energy* **2**, 16215 (2017).
- 476 7. S Boukhalifa, et al., In situ small angle neutron scattering revealing ion sorption in microporous  
477 carbon electrical double layer capacitors. *ACS Nano* **8**, 2495–2503 (2014) PMID: 24547779.
- 478 8. R Futamura, et al., Partial breaking of the coulombic ordering of ionic liquids confined in  
479 carbon nanopores. *Nat. Mater.* **16**, 1225–1232 (2017).
- 480 9. J Chmiola, et al., Anomalous increase in carbon capacitance at pore sizes less than 1  
481 nanometer. *Science* **313**, 1760–1763 (2006).
- 482 10. C Merlet, et al., Highly confined ions store charge more efficiently in supercapacitors. *Nat.*  
483 *Commun.* **4**, 2701 (2013).
- 484 11. S Kondrat, P Wu, R Qiao, AA Kornyshev, Accelerating charging dynamics in subnanometre  
485 pores. *Nat. Mater.* **13**, 387–393 (2014).
- 486 12. H Shao, YC Wu, Z Lin, PL Taberna, P Simon, Nanoporous carbon for electrochemical capac-  
487 itive energy storage. *Chem. Soc. Rev.* **49**, 3005–3039 (2020).
- 488 13. M Müller, B Kastening, The double layer of activated carbon electrodes: Part 1. the contribu-  
489 tion of ions in the pores. *J. Electroanal. Chem.* **374**, 149–158 (1994).
- 490 14. M Salanne, et al., Efficient storage mechanisms for building better supercapacitors. *Nat.*  
491 *Energy* **1**, 16070 (2016).
- 492 15. N Boon, R van Rooij, 'blue energy' from ion adsorption and electrode charging in sea and river  
493 water. *Mol. Phys.* **109**, 1229–1241 (2011).
- 494 16. RA Rica, R Ziano, D Salerno, F Mantegazza, D Brogioli, Thermodynamic relation between  
495 voltage-concentration dependence and salt adsorption in electrochemical cells. *Phys. Rev.*  
496 *Lett.* **109**, 156103 (2012).
- 497 17. P Biesheuvel, R Zhao, S Porada, A [van der Wal], Theory of membrane capacitive deioniza-  
498 tion including the effect of the electrode pore space. *J. Colloid Interface Sci.* **360**, 239–248  
499 (2011).
- 500 18. JP de Souza, MZ Bazant, Continuum theory of electrostatic correlations at charged surfaces.  
501 *The J. Phys. Chem. C* **124**, 11414–11421 (2020).
- 502 19. C Lian, S Zhao, H Liu, J Wu, Time-dependent density functional theory for the charging  
503 kinetics of electric double layer containing room-temperature ionic liquids. *The J. Chem.*  
504 *Phys.* **145**, 204707 (2016).
- 505 20. L Yang, BH Fishbine, A Migliori, LR Pratt, Molecular simulation of electric double-layer capac-  
506 itors based on carbon nanotube forests. *J. Am. Chem. Soc.* **131**, 12373–12376 (2009).
- 507 21. H Liu, CJ Jameson, S Murad, Molecular dynamics simulation of ion selectivity process in  
508 nanopores. *Mol. Simul.* **34**, 169–175 (2008).
- 509 22. RK Kalluri, D Konatham, A Striolo, Aqueous nacl solutions within charged carbon-slit pores:  
510 Partition coefficients and density distributions from molecular dynamics simulations. *The J.*  
511 *Phys. Chem. C* **115**, 13786–13795 (2011).
- 512 23. G Feng, PT Cummings, Supercapacitor capacitance exhibits oscillatory behavior as a func-  
513 tion of nanopore size. *The J. Phys. Chem. Lett.* **2**, 2859–2864 (2011).
- 514 24. C Hauf, M Woerner, T Elsaesser, Macroscopic electric polarization and microscopic electron  
515 dynamics: Quantitative insight from femtosecond x-ray diffraction. *Phys. Rev. B* **98**, 054306  
516 (2018).
- 517 25. T Sun, et al., Rapid electron transfer by the carbon matrix in natural pyrogenic carbon. *Nat.*  
518 *Commun.* **8**, 14873 (2017).
- 519 26. C Merlet, et al., Simulating supercapacitors: Can we model electrodes as constant charge  
520 surfaces? *The J. Phys. Chem. Lett.* **4**, 264–268 (2013) PMID: 26283432.
- 521 27. SA Evlashin, et al., Role of nitrogen and oxygen in capacitance formation of carbon nanowalls.  
522 *The J. Phys. Chem. Lett.* **11**, 4859–4865 (2020) PMID: 32515198.
- 523 28. G Hartmann, GS Hwang, First-principles description of electrocatalytic characteristics of  
524 graphene-like materials. *The J. Chem. Phys.* **153**, 214704 (2020).
- 525 29. T Hussain, E Olsson, K Alhameedi, Q Cai, A Karton, Functionalized two-dimensional  
526 nanoporous graphene as efficient global anode materials for li-, na-, k-, mg-, and ca-ion  
527 batteries. *The J. Phys. Chem. C* **124**, 9734–9745 (2020).
- 528 30. A Maslechko, T Verstraelen, TS van Erp, E Riccardi, Multiscale partial charge estimation on  
529 graphene for neutral, doped and charged flakes. *Phys. Chem. Chem. Phys.* **20**, 20678–20687  
530 (2018).
- 531 31. D Ibrahim Abouelamaiem, et al., New insights into the electrochemical behaviour of porous  
532 carbon electrodes for supercapacitors. *J. Energy Storage* **19**, 337–347 (2018).
- 533 32. ME Suss, et al., Impedance-based study of capacitive porous carbon electrodes with hierar-  
534 chical and bimodal porosity. *J. Power Sources* **241**, 266–273 (2013).
- 535 33. F Béguin, V Presser, A Balducci, E Frackowiak, Carbons and electrolytes for advanced super-  
536 capacitors. *Adv. Mater.* **26**, 2219–2251 (2014).
- 537 34. J Segalini, B Daffos, P Taberna, Y Gogotsi, P Simon, Qualitative electrochemical impedance  
538 spectroscopy study of ion transport into sub-nanometer carbon pores in electrochemical double  
539 layer capacitor electrodes. *Electrochimica Acta* **55**, 7489–7494 (2010).
- 540 35. J Pikunic, et al., Structural modeling of porous carbons: Constrained reverse monte carlo  
541 method. *Langmuir* **19**, 8565–8582 (2003).
- 542 36. SK Jain, RJM Pellenq, JP Pikunic, KE Gubbins, Molecular modeling of porous carbons using  
543 the hybrid reverse monte carlo method. *Langmuir* **22**, 9942–9948 (2006) PMID: 17106983.
- 544 37. C Bousige, A Bojan, FJ Ulm, RJM Pellenq, B Coasne, Optimized molecular reconstruction  
545 procedure combining hybrid reverse monte carlo and molecular dynamics. *The J. Chem.*  
546 *Phys.* **142**, 114112 (2015).
- 547 38. C Prehal, et al., A carbon nanopore model to quantify structure and kinetics of ion electro-  
548 sorption with in situ small-angle x-ray scattering. *Phys. Chem. Chem. Phys.* **19**, 15549–15561  
549 (2017).
- 550 39. H Sun, Compass: An ab initio force-field optimized for condensed-phase applications  
551 overview with details on alkane and benzene compounds. *The J. Phys. Chem. B* **102**, 7338–  
552 7364 (1998).
- 553 40. MJ McQuaid, H Sun, D Rigby, Development and validation of compass force field parameters  
554 for molecules with aliphatic azide chains. *J. Comput. Chem.* **25**, 61–71 (2004).
- 555 41. AB Bogeat, Understanding and tuning the electrical conductivity of activated carbon: A state-  
of-the-art review. *Critical Rev. Solid State Mater. Sci.* **0**, 1–37 (2019).
42. N Ganfoud, et al., Effect of the carbon microporous structure on the capacitance of aqueous  
supercapacitors. *Energy Storage Mater.* **21**, 190–195 (2019).
43. CG Gray, PJ Stiles, Nonlinear electrostatics: the poisson boltzmann equation. *Eur. J. Phys.*  
**39**, 053002 (2018).
44. AM Smith, AA Lee, S Perkin, The electrostatic screening length in concentrated electro-  
lytes increases with concentration. *The J. Phys. Chem. Lett.* **7**, 2157–2163 (2016) PMID:  
27216986.
45. T Verkholyak, A Kuzmak, S Kondrat, Capacitive energy storage in single-file pores: Exactly  
solvable models and simulations. *The J. Chem. Phys.* **155**, 174112 (2021).
46. X Li, et al., Water splitting: From electrode to green energy system. *Nano-Micro Lett.* **12**, 131  
(2020).
47. F Barzegar, et al., Investigation of different aqueous electrolytes on the electrochemical per-  
formance of activated carbon-based supercapacitors. *RSC Adv.* **5**, 107482–107487 (2015).
48. E Frackowiak, *Electrode Materials with Pseudocapacitive Properties*. (John Wiley and Sons,  
Ltd), pp. 207–237 (2013).
49. D Flévit, S Elias, J Hautman, Number of water molecules coupled to the transport of sodium,  
potassium and hydrogen ions via gramicidin, nonactin or valinomycin. *Biochim Biophys Acta.*  
**512**, 436–451 (1978).
50. JK Brennan, KT Thomson, KE Gubbins, Adsorption of water in activated carbons: Effects of  
pore blocking and connectivity. *Langmuir* **18**, 5438–5447 (2002).
51. D Ebrahimi, RJM Pellenq, AJ Whittle, Nanoscale elastic properties of montmorillonite upon  
water adsorption. *Langmuir* **28**, 16855–16863 (2012).
52. G Cassone, F Creazzo, PV Giaquinta, F Saija, A Marco Saitta, Ab initio molecular dynamics  
study of an aqueous nacl solution under an electric field. *Phys. Chem. Chem. Phys.* **18**,  
23164–23173 (2016).
53. R Mancinelli, A Botti, F Bruni, MA Ricci, AK Soper, Hydration of sodium, potassium, and  
chloride ions in solution and the concept of structure maker/breaker. *The J. Phys. Chem. B*  
**111**, 13570–13577 (2007) PMID: 17988114.
54. L Liu, PL Taberna, B Dunn, P Simon, Future directions for electrochemical capacitors. *ACS*  
*Energy Lett.* **0**, 4311–4316 (0).
55. R Ranganathan, S Rokkam, T Desai, P Koblinski, Generation of amorphous carbon models  
using liquid quench method: A reactive molecular dynamics study. *Carbon* **113**, 87–99  
(2017).
56. ACT van Duijn, S Dasgupta, F Lorant, WA Goddard, Reaxff: A Reactive Force Field for Hy-  
drocarbons. *The J. Phys. Chem. A* **105**, 9396–9409 (2001).
57. HJC Berendsen, JR Grigera, TP Straatsma, The missing term in effective pair potentials. *The*  
*J. Phys. Chem.* **91**, 6269–6271 (1987).